Twist-induced preferential distribution of dopants in single-crystalline Si nanowires

Xing-Ju Zhao,[1,2] Gotthard Seifert,[3] Junyi Zhu,[4,*] and Dong-Bo Zhang[2,1,†]
[1]*Beijing Computational Science Research Center, Beijing 100193, China*
[2]*College of Nuclear Science and Technology, Beijing Normal University, Beijing 100875, China*
[3]*Theoretische Chemie, Technische Universitat Dresden, Dresden D-01062, Germany*
[4]*Department of Physics, the Chinese University of Hong Kong, Hong Kong, China*

(Received 4 September 2019; revised manuscript received 6 November 2019; published 27 November 2019)

The distribution of dopants has significant influence on the electronic property of semiconductors. However, in a homogeneous crystalline material, the occupation of dopants is usually randomly distributed. Using the generalized Bloch theorem, we show that a twisting deformation has a pronounced impact on the distribution of dopants in single-crystalline Si nanowires (SiNWs). With systematic calculations, we find that the dopant atoms with smaller sizes than the host Si atom prefer atomic sites near the NW core, while dopants of larger sizes are prone to staying around the NW surface. The underlying mechanism of this intriguing phenomenon is related to the inhomogeneous shear strain along the NW radial direction. Such a trend is nearly independent of dopants with different numbers of valence electrons and also independent of the detailed crystal structures of NWs. Our findings provide an effective approach to control the dopant distribution in semiconductors, which is critical for the design of devices with reproducible electronic properties.

DOI: 10.1103/PhysRevB.100.174202

I. INTRODUCTION

Si nanowires (SiNWs) [1–4] and other semiconductor NWs [5–8] are structures that are appealing as building blocks of next generation nanodevices [3,9,10]. Recent experimental efforts have illustrated the possibility to grow this category of single-crystalline nanostructures [11,12], and to readily incorporate various dopants during the growth. For doping, not only is a high dopant density needed for an optimal performance of NWs for electronic applications, but also a controllable dopant distribution stands for an important parameter to tune the characteristic of semiconducting electrons [13].

Sufficient dopant concentration usually requires a low doping formation energy (E_f) such that the doped system is energetically stable. E_f is determined by the atomic size and the electronic environment of the dopants. If the dopant matches well the electronic environment of the host atom, the resultant E_f can be low. In addition, if the size mismatch is significant, a local deformation around the doping site can be induced, adding a large strain energy penalty to E_f. Therefore, choosing a dopant with a similar size as the host atom or applying uniaxial/biaxial strains to the host system is effective to release the strain energy and thus to obtain a reduced E_f [14].

Theoretically, an accurate evaluation of E_f can be realized by carrying out atomistic simulations such as first-principles calculations. Here it is interesting to note that in order to determine the optimal E_f, only a few atomic sites inside the crystal unit cell need to be considered for a substitutional dopant. This rule is still applicable even when uniaxial/biaxial strains are exerted [14]. This is because that due to the translational symmetry, crystals are structurally homogeneous (i.e., all lattice sites are energetically equivalent). This feature thus indicates that the occupation site of a substitutional dopant is essentially random in a homogeneous system. This leads to an interesting question: How to manipulate the occupation side of dopants in materials? This can be realized by introducing inhomogeneity to the system. For example, in NWs, due to the finite-size effect and surface effect, lattice sites along the NW radial direction are not energetically equivalent any longer [15–17]. As a result, dopants exhibits preferences for occupation sites. Indeed, first-principles calculations reveal that there is a tendency for the dopant to reside within the NW core or near the NW surface; experimental results also reveal that the distribution of dopants along the SiNW radial direction is nonuniform [15–17]. However, as the NW size increases, the finite-size effect and surface effect become less important and the occupation preference of dopants vanishes [18].

An alternative strategy is strain engineering [19–22]. For example, in a NW, a twisting deformation can invoke structural inhomogeneity with a strain gradient along the NW radial direction. Thus, E_f might be different for a dopant occupying different atomic sites along the NW radial direction. Indeed, an analytical bond-orbital analysis indicates that in SiNWs made from tetrahedral Si, dopants display a size-sensitive occupation preference [13]. However, a dopant usually is of a different number of valence electrons from the host Si atom. Thus, the extra charge (electron or hole) overlooked by the bond-orbital approach may play a role in the formation of E_f. More critical, it is unclear yet that whether the occupation preference of dopant revealed in tetrahedral SiNWs also applies for other crystal structures.

In this work, we investigate systematically the distribution of dopants in twisted SiNWs. Tetrahedral and hexagonal

*jyzhu@phy.cuhk.edu.hk
†dbzhang@bnu.edu.cn

SiNWs doped with elements from main groups IIIA, IVA, and VA with different atomic sizes are considered. For each NW, multiple crystallographic directions of growing are considered, e.g., for tetrahedral SiNWs, both fcc[211] and fcc[111] directions are considered, while for hexagonal SiNWs, both hcp[0001] and hcp[11$\bar{2}$0] directions are considered.

II. METHODS

We employ density-functional theory based first-principles approaches [23] as implemented in VASP [24] to study the formation energy and the lattice stress of doped bulk Si. The interactions of the valence electrons with the ionic cores are described by the projector augmented wave (PAW) [25] method. For the exchange-correlation functional, we use the generalized gradient approximation of Perdew, Burke, and Ernzerhof [26]. Si($4 \times 4 \times 4$) supercells are used to simulate the doped bulk Si. A $7 \times 7 \times 7$ k-point mesh and an energy cutoff of 500 eV are adopted. The electronic iteration was converged to 10^{-5} eV and the structures were fully relaxed by the conjugate gradient method until all the residual force components were less than 0.01 eV/Å. All these parameters have been carefully examined to ensure good convergence.

For twisted NWs, we instead employ the generalized Bloch theorem as coupled with the self-consistent charge density-functional tight-binding (scc-DFTB) [27,28] method. Because the translational symmetry of a NW is broken by the twist deformation, the traditional methods relying on translational periodic boundary condition are no longer applicable. In the generalized Bloch theorem, we describe the twisted NW structure with a helical symmetry,

$$\mathbf{X}_{\lambda,l} = \mathbf{R}^{\lambda}(\Omega)\mathbf{X}_{0,l} + \lambda\mathbf{T}, \tag{1}$$

where $\mathbf{X}_{0,l}$ ($l = 1, \ldots, N$) represents atoms inside the unit cell, λ denotes the sequence of the translational replica of the unit cell, and $\mathbf{X}_{\lambda,l}$ represents atoms inside the λth replica of the unit cell. The axial vector $\mathbf{T}$ and rotation vector $\mathbf{R}$ with rotation angle Ω are used to depict the NW screw. The electronic states under such helical boundary conditions are described in terms of generalized Bloch functions [27,28], with which the optimal NW geometry and energy can be obtained through full structural relaxation at arbitrary $\mathbf{T}$ and Ω. With this, we define a twist rate $\gamma = \Omega/|\mathbf{T}|$, which denotes the rotation angle per nanometer.

III. RESULTS

A. Formation energy of various dopants in tetrahedral Si

In bulk, the doping formation energy is defined as [29,30]

$$E_f = E_{\text{tot}} - E_0 + \mu_{\text{Si}} - \mu_{\text{D}}, \tag{2}$$

where E_{tot} and E_0 are the total energies of the doped and pristine systems, respectively. μ_{Si} and μ_{D} are the chemical potential of Si and the dopant, respectively. Using first-principles calculations, the formation energy E_f of a series of dopants are summarized in Table I. We also calculated the resulting stress σ and the bond length b_{D} between dopant and Si. Overall, for all the considered dopants, E_f are relatively low.

We focus on the size effect on E_f. Generally, if the size of a dopant is similar with that of an Si atom, b_{D} will be close to the Si-Si bond length ($b_{\text{Si}} = 2.37$ Å), and thus σ will be small. From Table I, compared to other dopants, Ge has a $b_{\text{Ge}} = 2.41$Å, closest to b_{Si}. Meanwhile, σ for Ge is also smallest.

TABLE I. Doping formation energy E_f, lattice stress σ, and bond length between dopants and Si b_{D}.

	E_f (eV)	σ (GPa)	b_{D} (Å)
B_{Si}	0.76	−0.62	2.10
C_{Si}	1.47	−0.84	2.03
N_{Si}	1.60	−0.87	2.05
Al_{Si}	0.98	0.19	2.42
Ge_{Si}	0.10	0.11	2.41
Sb_{Si}	1.07	0.34	2.58

A stress indicates a strain energy induced by the structural deformation around the dopant, which contributes to the formation energy E_f. Therefore, it is reasonable to expect a relatively low E_f given a small σ. This is completely supported by the data in Table I.

It is more interesting to notice that if $b_{\text{D}} < b_{\text{Si}}$ (i.e., the dopant size is smaller than that of Si), σ will be negative; otherwise, σ will be positive. This hints that a dopant with a larger size needs larger space to lower the formation energy E_f. That is, for a dopant with positive σ, E_f will be lowered if a tensile strain is applied; On the other hand, for a dopant with negative σ, E_f will be lowered if a compressive strain is applied. This property provides a straightforward route to modulate the distribution of dopants by invoking inhomogeneous strains where dopants with smaller (larger) size will prefer to locate at regions with compressive (tensile) strain in order to lower E_f.

We note that this strategy can be extended to inhomogeneous shear strain. A shear strain in the linear elastic regime alters neither the bond length between atoms nor the atomic space in solids. However, the situation changes if the shear strain is beyond the linear regime, which is often encountered in the strain engineering of materials. In the following, we show that a twist applied to a NW that induces inhomogeneous shear strain in the NW radial direction has strong modulation on the occupation location of dopants.

B. Formation energy of various dopants in twisted SiNWs

For the tetrahedral [100] SiNW, we consider different dopants including B, C, N, Al, Ge, and Sb. Note that due to the deep energy levels of C and N, it is more proper to treat them as impurities. For each dopant, several doping sites [$n = 0, \ldots 6$ in Fig. 1(a)] along the NW radius are examined. The total energy of a dopant at site n is labeled as E_n. Using the energy for dopant at site 0 (E_0) as a reference, we obtain the relative formation energy as $E_n - E_0$. The twisted configuration of the SiNW is shown in Fig. 1(b). Results of $E_n - E_0$ as function of twist rate γ are shown in Figs. 1(c) and 1(d).

For undistorted NW, i.e., $\gamma = 0$, $E_n - E_0$ remains to zero for all considered atomic sites. This demonstrates an energetic equivalence for these sites, in spite of the small size of the SiNW (with a diameter of about 4 nm in Fig. 1). Thus, the size effect such as surface effect should be negligible for $E_n - E_0$.

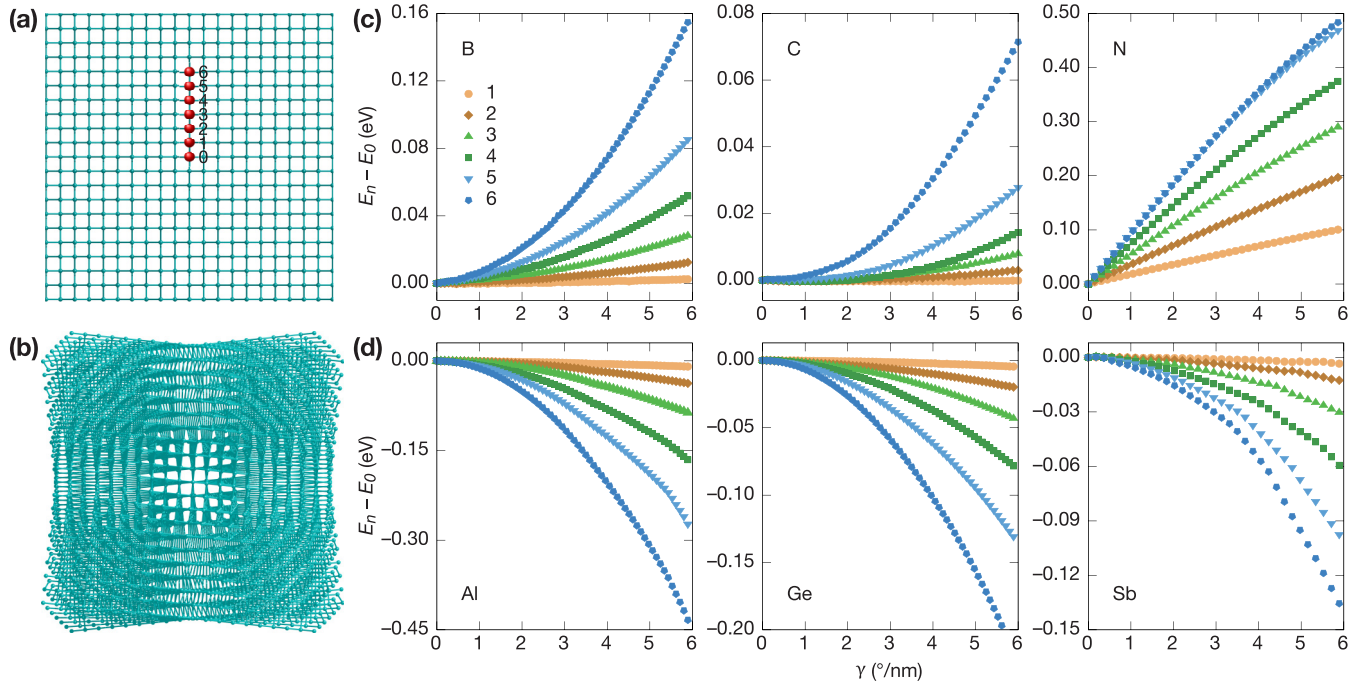

FIG. 1. Relative energy of various doped configurations in twisted SiNWs. (a), (b) Axial view of the tetrahedral pristine (a) and twisted (b) Si[100] NWs with a diameter of about 4 nm; the filled red ball and its corresponding number in (a) indicate the atomic sites of various dopants. (c), (d) Relative energy as a function of the twist rate γ of various dopants located at different atomic sites marked in (a).

Under twisting, $E_n - E_0$ displays an interesting trend. For impurities of B, C, and N, for each impurity site n, $E_n - E_0$ increases with γ, and at a given γ, $E_n - E_0$ is higher for the site closer to the NW surface, Fig. 1(c). This hints that in the twisted SiNW, these dopants or impurities prefer to occupy atomic sites near the NW core, while Al, Ge, and Sb do the reverse. For each doping site, $E_n - E_0$ decreases with γ, and at a given γ, $E_n - E_0$ is lower for the site closer to the NW surface, Fig. 1(d). This hints that in the twisted SiNW, these dopants prefer to occupy atomic sites near the NW surface.

We attribute such distinct responses to the different atomic sizes of dopants. B, C, and N atoms have atomic sizes smaller than Si atom while Al, Ge, and Sb are of larger atomic size than Si atom. The underlying mechanism of this size dependence can be understood by exploring the twist-induced structural distortion. Twisting induces an inhomogeneous shear strain along the NW radial direction [13]. Under such a strain field, the atomic sites along the NW radius are no longer equivalent. To characterize the strain effect on atoms, we evaluate the atomic volume for atomic site n:

$$V_n = \frac{4\pi}{3} R_n^3, \tag{3}$$

where $R_n = \frac{1}{2}\bar{d}_n$ is the half of the average bond length $\bar{d}_n$ between the referred atom at site n and its four nearest-neighbor Si atoms.

In Fig. 2, we show the variation of V_n along the radial direction in undistorted and twisted SiNW. For the undistorted SiNW, the atomic volume V_n of different sites almost remains invariant. This, again, reflects the equivalence between different sites. However, under twisting, V_n varies with site n. Figure 2 shows V_n increases monotonically with n at the twist rate of $\gamma = 6.3^\circ/\text{nm}$. Therefore, in a twisted SiNW, dopants or impurities of smaller size, such as B, C, and N, prefer to stay near the NW core where they match well with the environment (atomic space) such that the formation energy E_f is optimized. Similarly, for dopants with larger size, such as Al, Ge, and Sb, they shall stay adjacent to the NW surface to match the environment for an optimal E_f.

We note that B and Al possess three valence electrons while N and Sb have five valence electrons. Can the difference in valence electrons affect the preferential occupation of dopants in twisted SiNW? After all, the number of valence electrons are important for the covalent bonding in a

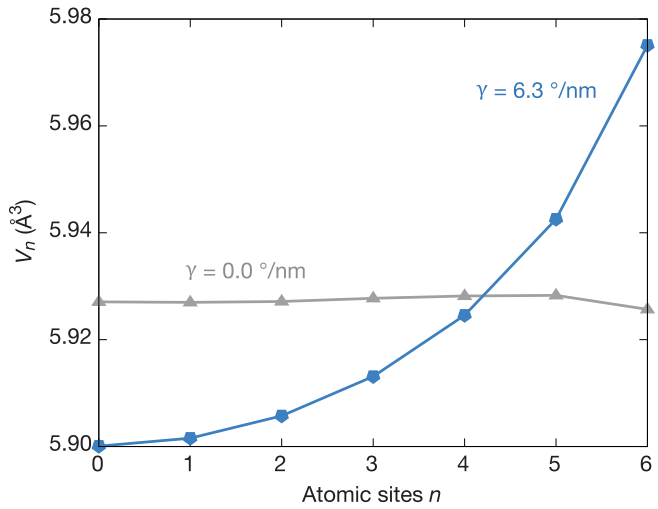

FIG. 2. Atomic volume V_n of different atomic sites along the radial direction of twisted and pristine crystalline Si[100] nanowires.

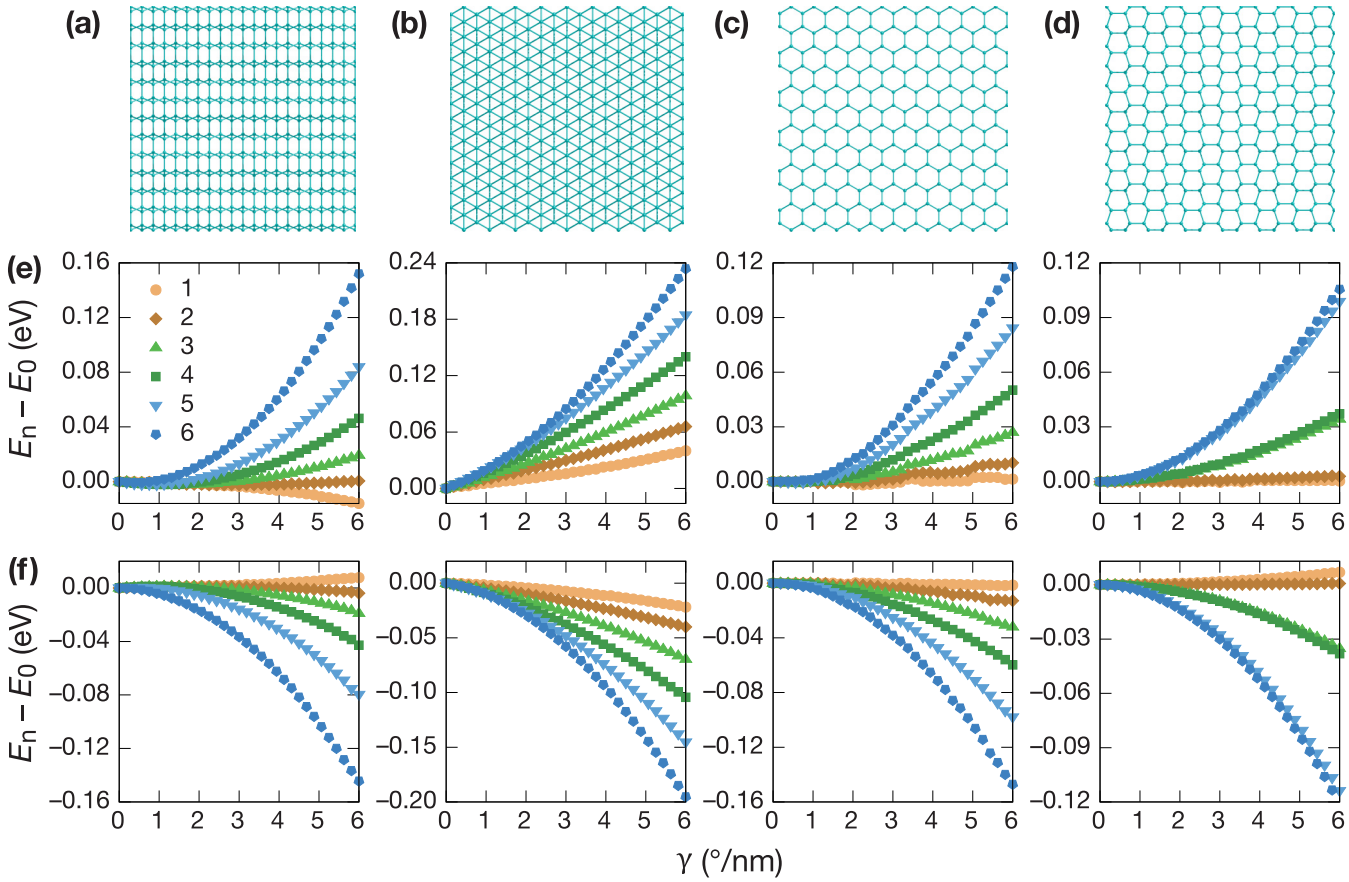

FIG. 3. Relative energy of exemplary dopants under various crystalline Si nanowires. (a)–(d) Axial view of Si fcc[211], fcc[111], hcp[0001], hcp[11$\bar{2}$0] nanowires, respectively. (e) Relative energy of B and (f) Ge doped configurations of each NW stacking forms, respectively.

semiconductor. Here, we want to clarify that this has little impact on the preferential occupation of dopants. First of all, we emphasize that the preferential occupation of dopants in twisted SiNW is due to the difference in atomic size of dopants. This can be inferred directly from the behavior of impurity C and dopant Ge, both of which have the same number of valence electrons with Si atom, such that the effect due to the difference in valence electrons can be ruled out. Second, focusing on the group of B, C, and N, the variation in the number of valence electrons does not alter the trend that dopants prefer to stay near the core of the twisted SiNW. This also hints that under twisting, the impact of the variation of the electronic environment on the dopant occupation is secondary, compared to the size effect. A similar situation can be also identified for Al, Ge, and Sb.

C. Occupation preference of dopants in various SiNWs under twisting

The above discussion completely confirms that the size of the dopant atoms dominates the distribution of dopants in twisted SiNWs. Can this occupation preference of dopant revealed in tetrahedral SiNWs be applied to other NWs with different crystal structures? Here, with B and Ge dopant atom as representative examples, we examine their most stable (with lower E_f) occupation sites in different SiNWs.

Truncated tetrahedral Si, a SiNW along the [211] direction, and a SiNW along the [111] direction are proposed; see Figs. 3(a) and 3(b), respectively. We have also considered SiNW with hexagonal-close-packed (hcp) lattice. Figures 3(c) and 3(d) show hcp SiNWs in [0001] and hcp[11$\bar{2}$0] directions, respectively.

For all these SiNWs under twisting, we have calculated $E_n - E_0$ for dopants at different atomic sites n. Results are summarized in Figs. 3(e) and 3(f). For B dopant, $E_n - E_0$ increases with twist rate γ and $E_n - E_0$ is higher when the doping site n is closer to the NW surface under a given twist rate, Fig. 3(e). On the other hand, for Ge dopant, $E_n - E_0$ decreases with twist rate γ and $E_n - E_0$ is lower when the doping site n is closer to the NW surface under a given twist rate, Fig. 3(f). These results indicate that B prefer to stay around the NW core while Ge will occupy the site adjacent to the NW surface in a twisted SiNW. It is clear that the trend is similar to that identified in tetrahedral SiNW. These results indicate that the occupation preference of dopants in twisted SiNWs is essentially dominated by the atomic size of dopants, regardless of the lattice structure.

IV. CONCLUSION

Using first-principles calculation and the generalized Bloch theorem implemented in scc-DFTB, we systematically

investigate the distribution of dopants in twisted SiNWs. Considering dopants from IIIA, IVA, and VA main groups elements with different atomic sizes, we show that the dopant atoms with smaller sizes than the host Si atom prefer atomic sites near the NW core, while dopants of larger sizes are prone to staying around the NW surface. The difference in valence electrons of dopants plays a negligible role. Such a trend is also independent of the lattice structure of SiNWs. The discussed twist strain can be exerted on SiNWs by state-of-the-art experimental techniques, such as nanofocused x-ray diffraction [21]. These findings pave a route to modulate the dopant distribution, which is critical for device design with reproducible electronic performance at nanoscale.

ACKNOWLEDGMENTS

This work was supported by Ministry of Science and Technology of China under Grant No. 2017YFA0303400, NSFC under Grants No. 11674022 and No. U1930402, and the Postdoctoral Innovative Talents Support Program (Grant No. BX201700025). D.-B.Z. was supported by the Fundamental Research Funds for the Central Universities. J.Z. was supported by start-up funding, Hong Kong Research Grant Council funding (Grant No. 14319416), and direct grants (Grants No. 4053233, No. 4053134, and No. 3132748) at the Chinese University of Hong Kong. Simulations were performed at Beijing Computational Science Research Center and the Sugon TC5600 supercomputing system.

[1] Y. Cui, X. Duan, J. Hu, and C. M. Lieber, Doping and electrical transport in silicon nanowires, J. Phys. Chem. B **104**, 5213 (2000).

[2] Y. Cui and C. M. Lieber, Functional nanoscale electronic devices assembled using silicon nanowire building blocks, Science **291**, 851 (2001).

[3] C. K. Chan, H. Peng, G. Liu, K. McIlwrath, X. F. Zhang, R. A. Huggins, and Y. Cui, High-performance lithium battery anodes using silicon nanowires, Nat. Nanotechnol. **3**, 31 (2007).

[4] A. I. Hochbaum, R. Chen, R. D. Delgado, W. Liang, E. C. Garnett, M. Najarian, A. Majumdar, and P. Yang, Enhanced thermoelectric performance of rough silicon nanowires, Nature (London) **451**, 163 (2008).

[5] X. Duan, Y. Huang, Y. Cui, J. Wang, and C. M. Lieber, Indium phosphide nanowires as building blocks for nanoscale electronic and optoelectronic devices, Nature (London) **409**, 66 (2001).

[6] Z. Zhong, F. Qian, D. Wang, and C. M. Lieber, Synthesis of *p*-type gallium nitride nanowires for electronic and photonic nanodevices, Nano Lett. **3**, 343 (2003).

[7] B. D. Yuhas, D. O. Zitoun, P. J. Pauzauskie, R. He, and P. Yang, Transition-metal doped zinc oxide nanowires, Angew. Chem. **118**, 434 (2006).

[8] C. Liu, J. Sun, J. Tang, and P. Yang, Zn-doped *p*-type gallium phosphide nanowire photocathodes from a surfactant-free solution synthesis, Nano Lett. **12**, 5407 (2012).

[9] A. I. Hochbaum and P. Yang, Semiconductor nanowires for energy conversion, Chem. Rev. **110**, 527 (2010).

[10] B. Tian, T. J. Kempa, and C. M. Lieber, Single nanowire photovoltaics, Chem. Soc. Rev. **38**, 16 (2009).

[11] Y. Cui, L. J. Lauhon, M. S. Gudiksen, J. Wang, and C. M. Lieber, Diameter-controlled synthesis of single-crystal silicon nanowires, Appl. Phys. Lett. **78**, 2214 (2001).

[12] A. M. Morales and C. M. Lieber, A laser ablation method for the synthesis of crystalline semiconductor nanowires, Science **279**, 208 (1998).

[13] D.-B. Zhang, X.-J. Zhao, G. Seifert, K. Tse, and J. Zhu, Twist-driven separation of *p*-type and *n*-type dopants in single crystalline nanowires, Natl. Sci. Rev. **6**, 532 (2019).

[14] J. Zhu, F. Liu, G. B. Stringfellow, and S.-H. Wei, Strain-Enhanced Doping in Semiconductors: Effects of Dopant Size and Charge State, Phys. Rev. Lett. **105**, 195503 (2010).

[15] J. Han, T.-L. Chan, and J. R. Chelikowsky, Quantum confinement, core level shifts, and dopant segregation in *p*-doped Si⟨110⟩ nanowires, Phys. Rev. B **82**, 153413 (2010).

[16] M.-F. Ng, M. B. Sullivan, S. W. Tong, and P. Wu, First-principles study of silicon nanowire approaching the bulk limit, Nano Lett. **11**, 4794 (2011).

[17] H. Peelaers, B. Partoens, and F. M. Peeters, Formation and segregation energies of B and P doped and BP codoped silicon nanowires, Nano Lett. **6**, 2781 (2006).

[18] C. R. Leao, A. Fazzio, and A. J. R. da Silva, Confinement and surface effects in B and P doping of silicon nanowires, Nano Lett. **8**, 1866 (2008).

[19] T. Cohen-Karni, L. Segev, O. Srur-Lavi, S. R. Cohen, and E. Joselevich, Torsional electromechanical quantum oscillations in carbon nanotubes, Nat. Nanotechnol. **1**, 36 (2006).

[20] A. M. Fennimore, T. D. Yuzvinsky, W.-Q. Han, M. S. Fuhrer, J. Cumings, and A. Zettl, Rotational actuators based on carbon nanotubes, Nature (London) **424**, 408 (2003).

[21] J. Wallentin, D. Jacobsson, M. T. Osterhoff, Markus, Borgstrom, and T. Salditt, Bending and twisting lattice tilt in strained core-shell nanowires revealed by nanofocused x-ray diffraction, Nano Lett. **17**, 4143 (2017).

[22] I. Popov, S. Gemming, S. Okano, N. Ranjan, and G. Seifert, Electromechanical switch based on Mo_6S_6 nanowires, Nano Lett. **8**, 4093 (2008).

[23] P. Hohenberg and W. Kohn, Inhomogeneous electron gas, Phys. Rev. **136**, B864 (1964).

[24] G. Kresse and J. Hafner, Ab initio molecular-dynamics simulation of the liquid-metal–amorphous-semiconductor transition in germanium, Phys. Rev. B **49**, 14251 (1994).

[25] P. E. Blöchl, Projector augmented-wave method, Phys. Rev. B **50**, 17953 (1994).

[26] J. P. Perdew, K. Burke, and M. Ernzerhof, Generalized Gradient Approximation Made Simple, Phys. Rev. Lett. **77**, 3865 (1996).

[27] D.-B. Zhang and S.-H. Wei, Inhomogeneous strain-induced half-metallicity in bent zigzag graphene nanoribbons, npj Comput. Mater. **3**, 32 (2017).

[28] L. Yue, G. Seifert, K. Chang, and D.-B. Zhang, Effective zeeman splitting in bent lateral heterojunctions of graphene and hexagonal boron nitride: A new mechanism towards half-metallicity, Phys. Rev. B **96**, 201403(R) (2017).

[29] S. Limpijumnong, S. B. Zhang, S.-H. Wei, and C. H. Park, Doping by Large-Size-Mismatched Impurities: The Microscopic Origin of Arsenic- or Antimony-Doped *p*-Type Zinc Oxide, Phys. Rev. Lett. **92**, 155504 (2004).

[30] S. B. Zhang and J. E. Northrup, Chemical Potential Dependence of Defect Formation Energies in GaAs: Application to Ga Self-Diffusion, Phys. Rev. Lett. **67**, 2339 (1991).